

Macro-Mechanical behavior of unique surface welded joints (AA5083) utilizing tungsten inert gas welding against single-stage homogenization annealing

Muhammad Muzamil^{a,✉}, Jianjun Wu^{b,✉}, Muhammad Samiuddin^{c,d}, Arfan Majeed^b,
Sumair Uddin Siddiqui^d, Muhammad Mudassir^e

^aMechanical Engineering Department, NED University of Engineering and Technology, Karachi 75270, Pakistan

^bSchool of Mechanical Engineering, Northwestern Polytechnical University, 127 West Youyi Road, Xi'an, Shaanxi 710072, PR China

^cMetallurgical Engineering Department, NED University of Engineering and Technology, Karachi 75270, Pakistan

^dState Key Laboratory of Solidification Processing, Northwestern Polytechnical University, Xi'an 710072, PR China

^eDepartment of Chemistry, NED University of Engineering and Technology, Karachi 75270, Pakistan

(✉Corresponding author: wujj@nwpu.edu.cn; muzamil@neduet.edu.pk)

Submitted: 22 March 2020; Accepted: 4 August 2020; Available On-line: 15 October 2020

ABSTRACT: Surface welded joints are considered an advance and innovative strategy to achieve acceptable strength without consuming much energy on specimen preparation. Two surfaces of AA5083 plates were welded from four sides using the same filler material to prepare specimens. In the surface joint analysis, up to 2–2.2 mm fusion depth was achieved on each side, though the central portion remained characteristically unfused. After joining, homogenization annealing has been performed at 275 °C and 325 °C to hold the specimens for 3 h, which increased the joint performance up to 57.6%. The optical micrographs of fused zones have outlined the alternative-combine visibility of Al₆(Mn,Fe) and Mg₂Si in analysis with the increase in annealing temperature from 275 °C to 325 °C. Observations from fracture surface characteristics include *completely fused zone* (CFZ) and *base material-fused zone* (BMFZ) interface boundary, which in combination defined the whole mechanism of fracture.

KEYWORDS: AA5083 alloys; Homogenization; Mechanical behavior; Surface weld; Tungsten inert gas welding

Citation/Citar como: Muzamil, M.; Wu, J.; Samiuddin, M.; Majeed, A.; Uddin Siddiqui, S.; Mudassir, M. (2020). "Macro-Mechanical behavior of unique surface welded joints (AA5083) utilizing tungsten inert gas welding against single-stage homogenization annealing". *Rev. Metal.* 56(3): e173. <https://doi.org/10.3989/revmetalm.173>

RESUMEN: *Comportamiento macromecánico de uniones soldadas de superficie (AA5083) utilizando soldadura con gas inerte de tungsteno con recocido de homogeneización en una sola etapa.* Las uniones soldadas de superficie se consideran una estrategia avanzada e innovadora para lograr una resistencia aceptable sin consumir excesiva energía en la preparación de las muestras. Se soldaron dos superficies planas de la aleación AA5083 desde cuatro lados y utilizando el mismo material de relleno. En el análisis de la soldadura de superficie, se logró una profundidad de fusión de hasta 2 - 2,2 mm en cada lado, aunque la parte central permaneció sin fusionar. Después de la unión, se realizó un recocido de homogeneización a 275 y 325 °C durante 3 h, lo que aumentó el rendimiento de la unión hasta un 57,6%. Las micrografías ópticas de las zonas fusionadas han permitido la visibilidad de combinación alternativa de Al₆(Mn, Fe) y Mg₂Si con el aumento de la temperatura de recocido de 275 a 325 °C. Las observaciones de la superficie de la fractura incluyen el límite de la interface de la *zona completamente fusionada* (CFZ) y la *zona fusionada del material base* (BMFZ), que en combinación definieron todo el mecanismo de la fractura.

PALABRAS CLAVE: Aleaciones AA5083; Comportamiento mecánico; Homogeneización; Soldadura de superficie; Soldadura con gas inerte de tungsteno

ORCID ID: Muhammad Muzamil (<https://orcid.org/0000-0001-8380-0502>); Jianjun Wu (<https://orcid.org/0000-0001-6953-5511>); Muhammad Samiuddin (<https://orcid.org/0000-0002-2350-6114>); Arfan Majeed (<https://orcid.org/0000-0002-6835-7706>); Sumair Uddin Siddiqui (<https://orcid.org/0000-0002-9304-0700>); Muhammad Mudassir (<https://orcid.org/0000-0003-3108-5740>)

Copyright: © 2020 CSIC. This is an open-access article distributed under the terms of the Creative Commons Attribution 4.0 International (CC BY 4.0) License.

1. INTRODUCTION

Aluminum alloy AA5083 gained considerable attention in marine, automotive and aerospace industries due to their useful properties such as excellent formability, high strength, good corrosion resistance, and superb weldability. The pressure to produce light structures consumes low fuel, requires integration with preferable joining processes for aluminum alloys without any micro and macro defects, still relies on research and development work (Huang *et al.*, 2017; Baskutis *et al.*, 2019). This requirement has led to innovation in joint design considerations in real-time manufacturing systems.

In non-heat treatable aluminum alloys, work hardening is employed to improve further strength. However, the intrinsic hardening effect depends upon the availability of alloying elements (Mg, Mn, Fe, Si) that triggers the dispersion of phases and solid solution strengthening within the matrix. AA5083 alloy extensively utilized in the form of cooled rolled sheets in outer and inner structure panels of lightweight vehicles because of deep drawing and high stretch forming abilities. In most cases, homogenization annealing is the post process to stabilize the microstructure against excessive plastic deformations (Li *et al.*, 2013; Zhang *et al.*, 2017). Moreover, this alloys series is recommended for welding and limited references are available using solid-state friction stir welding (Bozzi *et al.*, 2010; Palanivel *et al.*, 2014). Although the overall reduction in mechanical properties is treated less critical for non-heat treatable in contrast to heat-treatable aluminum alloys (Kumar and Sundarajan, 2009). Among various parameters of TIG welding heat input is the main process parameter that affects the mechanical properties of the welded joint (Vargas-Arista *et al.*, 2019; Samiuddin *et al.*, 2020). Results propose from tungsten inert gas (TIG) arc welding provides new ways of feasibility and for comparison purposes, which still seems to be a vacant space for this alloy from a research perspective.

AA5083 is fundamentally recognized as a marine-grade weldable alloy for frequent ascertain structural applications. The welded joints become easy stress concentration points in these types of severe naval conditions and harsh environments. However, for the prevention of any premature failure that will become ultimately responsible for the overall structural collapse, it is classically recommended to adopt post-treatments to gain up trust in weld strength. Engler *et al.* (2017) have presented a comprehensive study on homogenization annealing of AA5754 and AA5182 (with a difference in Mg contents) at 545 °C and 530 °C respectively. The extracted samples from as-cast ingot after annealing have shown a significant impact on mechanical properties. Distinguish studies on AA5083 are available in literature conquering

the mechanical properties from different aspects through the execution of homogenization annealing (Chen *et al.*, 2015; Huang *et al.*, 2016; Engler and Miller-Jupp, 2016; Dolić and Brodarac, 2017). In a similar scenario, it is accepted that the appropriate selection of the homogenization cycle may improve the microstructural behavior of welded specimens.

Another hefty concern in TIG welding is the selection of compatible filler with the base material, otherwise rapid occurrence of solidification cracking experiences in weldments due to high thermal stresses and solidification cavities formation (Chen *et al.*, 2015; Geng *et al.*, 2018). This situation is equally exasperation for both heat treatable and non-heat treatable aluminum alloys. High silicon contents fillers (ER4043, ER4047, ER4145) have captured the major proportion in contrast to other categories for its endorsed low crack susceptibility (Soysal and Kou, 2019). However, high Mg content base fillers (ER5654, ER5556, ER5356) are almost equally famous for domestic and industrial applications. The reason is to provide adequate strength to joints via the presence of Mg, which further support in solid solution strengthening and dispersion phase formations. The authors have recently contributed a study on the utilization of balanced heat treatable filler contents in-between Mg and Si (AA6061) on the non-heat treatable base material (AA5182) (Muzamil *et al.*, 2019a) using surface welded joints strategy. After age-hardening treatment, significant results towards mechanical behavior were achieved, which further motivated towards this presented work.

The vaporization of Mg contents against the high current values is acknowledged as a substantial issue leaving behind a low strength joint, that's why high Mg content filler (AA5083) is selected for examination in contrast to high Si-based fillers. In this presented study, a unique surface welded joints technique is considered to assess the joint strength using the TIG welding process. This approach will play a dynamic part in the modern designing of joints where welding process cost, efficiency, customer needs, and structural integrity desires to be achieved from available manufacturing infrastructure. In experimentations of surface joints, four sides of two separate halves are joined up to moderate interface depth of welds fused with the base material. A single-stage homogenization annealing cycle is executed on surface welded specimens, which is considerably more economically feasible than two-stage homogenization and artificial age-hardening treatment. The further presented objective is to uncover the macro-mechanical behavior of newly developed strategy and characterize the distinguish zones on fracture surfaces, which were created against filler deposition with the base material boundary interface.

2. MATERIALS AND EXPERIMENTAL PLAN

Commercially available AA5083 aluminum alloy plate of 12 mm in thickness, with nominal composition Mg 4.0-4.2, Mn 0.4-0.5, Fe 0.3-0.4, Si <0.2, Cu <0.2, Zn <0.1, Cr <0.1, Ti <0.05 and Zr <0.05 (wt%) was used in this study as the base material (BM). Direct profile of tensile specimens in two identical halves (P1 and P2) was fabricated ensuing ASTM E8/8M-11 guidelines comprise 50 mm gauge length and 12.5 mm width. OTC ACCUTIG 300P welding machine attached with manual treating torch was employed to weld the specimens. The two halves of specimens were surface welded from four sides (1, 2, 3 and 4) and allow the bead to solidify up to room temperature as represented in Fig. 1a. AA5083 is also used as the filler material, which was extracted in strips (2.5 mm-thick) from the BM plate. It is to be noted that no polishing and post-machining was done on the surface of the weld for tensile testing. All the tensile tests were conducted on CSS-4411 (China Mechanical Testing Equipment Co., Ltd., Changchun, PR China) universal tensile testing machine at a cross-head speed of $2.5 \text{ mm} \cdot \text{min}^{-1}$. The details of the utilized welding parameters of the process (Ahmadi *et al.*, 2017) are listed in Table 1.

Two groups of welded specimens of 200 mm in length were annealed in a preheating furnace at $275 \text{ }^\circ\text{C}$ and $325 \text{ }^\circ\text{C}$ for 3 hours respectively. All the annealed specimens were quenched in water at $40 \text{ }^\circ\text{C}$ temperature. The other group of specimens was just surface welded (un-annealed) for comparison purposes with homogenization annealing. Finally, the effect of homogenization annealing on joint strength behavior was determined by tensile testing. The average value of two tested specimens for each group arrangement was used to ensure the repeatability of results. The cross-sections of surface welded specimens depicted in Fig. 1b were subjected to fractured surface examination using TESCAN-VEGA3 scanning electron microscope

TABLE 1. Utilized parameters in tungsten inert gas (TIG) Welding Process

Selected parameter	Characteristic value
AC Current	160 Amp
Electrode diameter	Tungsten 3.2 mm
Shielding Gas	Argon
Gas flow rate	$20 \text{ lit} \cdot \text{min}^{-1}$
Frequency	80 Hz

(SEM). The guidelines from ASTM-E407-07 were imparted for microstructural analysis, which accommodates the sequential grinding on SiC papers (400#, 800#, 1000#, 1500#, and 2000#) pursued by polishing (diamond paste: 5, 2.5, 1 and $0.5 \mu\text{m}$) to obtain a scratch-free mirror surface. All the specimens were etched with a modified Keller solution (4 ml HF, 1 ml HCl, 1 ml HNO_3 and 35 ml H_2O), whereas Olympus (GX-71, Japan) was used to examine the microstructures of prepared specimens.

3. RESULTS AND DISCUSSION

In 5XXX series, homogenization annealing of cold-worked materials resulted in an equiaxed grain structure and transformation of precipitates into plate-like dispersoids (Ratchev *et al.*, 1995; Huh *et al.*, 2001; Xia *et al.*, 2014; Yi *et al.*, 2018). Moreover, the existence of primary eutectic particles formed during the solidification process was also confirmed (D'Antuono *et al.*, 2017). The lined-up annealing technique was utilized for improvement in joint strength considering a similar advantage for fusion surface joints. Figure 2 shows the engineering stress and strain curves plotted for $275 \text{ }^\circ\text{C}$ and $325 \text{ }^\circ\text{C}$ of homogenized annealing in comparison with the un-annealed sample (as surface-welded). In stress calculations, only fused area dimensions are considered which can be computed from cross-section

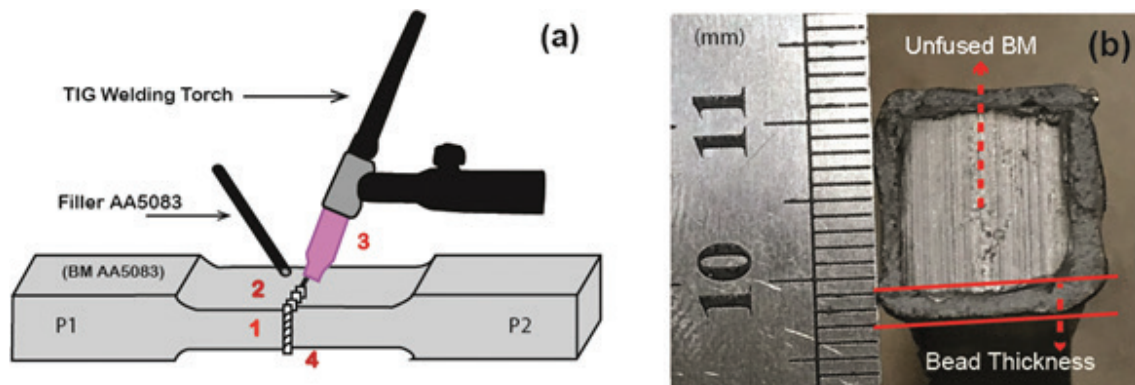


FIGURE 1. (a) Pictorial illustration of surface welded joints using TIG welding process, and (b) Cross-sectional view of fractured joint surface representing fused and unfused regions.

analysis as captured in Fig. 1b. The ultimate tensile strengths of TIG joints have depicted an increasing trend from 125, 162 to 197 MPa defining from un-annealed (as surface-welded) to 275 °C and 325 °C annealing temperature at constant holding time for 3 hours. The above-conferred results pointed out the increment of joint efficiency in terms of stress ratios between annealed and as surface-welded specimens. From the recorded experimental data, a 57.6% increment of joint efficiency is observed which is quite competitive for surface welded joint design. The mechanism involved in Al-Mg-Mn alloys for precipitates transformation against annealing cycles is solely responsible for this targeted achieved results (Engler and Miller-Jupp, 2016). This treatment has only transformed the precipitation structures, though the physical dimensions of all fused beads considered the same in the study. However, Fig. 3

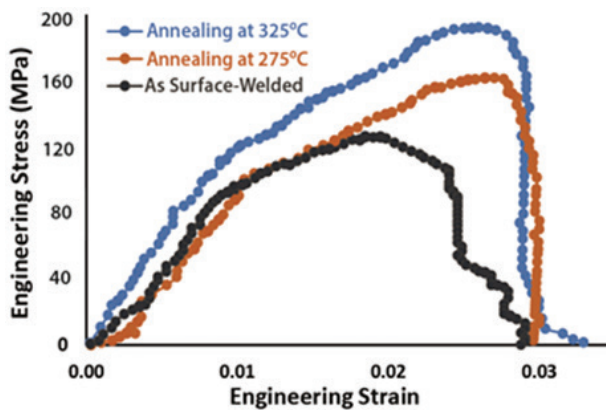


FIGURE 2. Stress-Strain curve of as surface-welded joint (un-annealed condition), and homogenize annealed at 275 °C and 325 °C.

represents the dimensional measurement across the width of gauge lengths at two points. The first point represented the dimension at the edge of gauge length and second at the extreme closure with the weld bead. It is to be noted copiously that a negligible change was occurred in-between two points for both homogenized and as-welded specimens, which is in compliance with the low engineering strains in Fig. 2. Hence, the overall applied load was endured by the surface welded joint specimens, and the values highlighted in Fig. 2 represents the actual stresses and strains of joint design. This technique may be considered equally fruitful for the assessment of joint strengths only, without taking into account of BM in the solicitation.

Figure 4(a-b) have shown the microstructures of the as-welded specimen, which discerned second phase particles that were formed during solidification of the weldment. As welding is considered a non-equilibrium process, thus solute gets lesser time to form precipitation consequently precipitation free zone (PFZ) developed as distinctly highlighted by yellow circles. Notably, the solubility of Mg in Al is around 2% at room temperature and increases to 14.9% when the temperature reaches to 450 °C. Therefore, a massive percentage of Mg remains dissolved in matrix and predominantly a single-phase must exist until and unless any non-equilibrium condition exhibits. However, the availability of Mg than its solubility limit will cause the emergence of a new phase within and around the parent phase matrix. In alloys with 3-4% Mg, Mg_2Si is usually formed (Engler *et al.*, 2017; D'Antuono *et al.*, 2017), other compounds such as Al_6Mn , Al_3Fe , $\alpha-Al(Fe,Mn)Si$, and other Al-Mg-Si intermetallic compounds have also been witnessed in structure (Radetić *et al.*, 2012; Engler and Miller-Jupp, 2016).

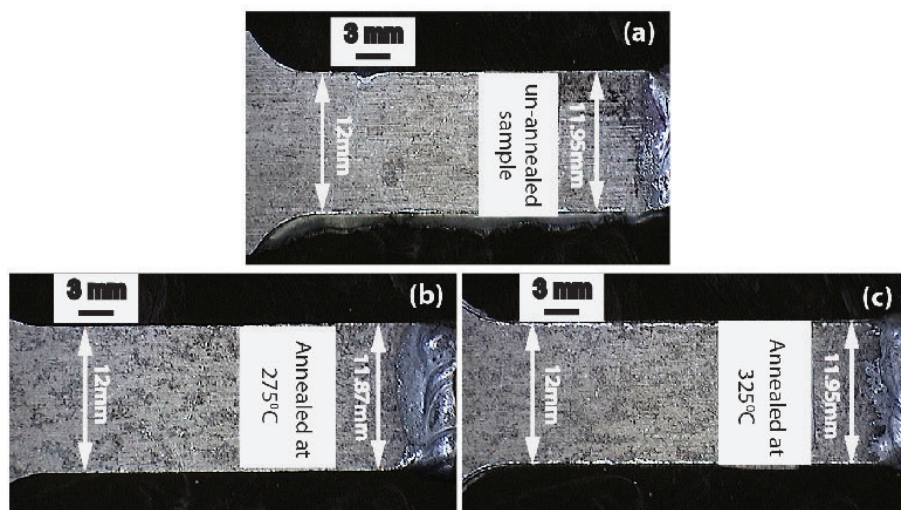


FIGURE 3. Dimensional measurement across the width of gauge length: (a) un-annealed sample, (b) annealed sample at 275 °C, and (c) annealed sample at 325 °C.

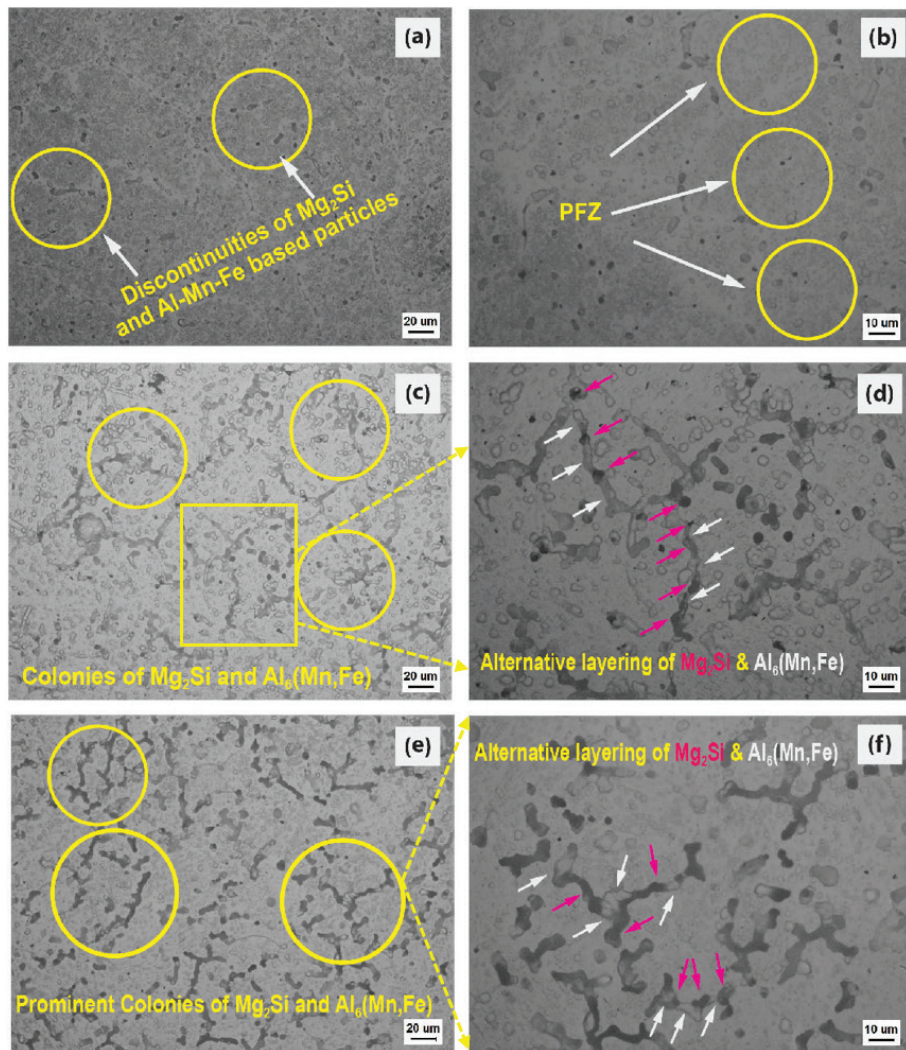


FIGURE 4. Optical micrographs (a-b) representing microstructure of un-annealed samples, (c-d) microstructures at 275 °C annealing temperature, (e-f) microstructures at 325 °C annealing temperature.

Moreover, Fig. 4(c-d) and 4(e-f) have represented the microstructures of a system that underwent a single-stage annealed cycle at 275 °C and 325 °C respectively. These microstructures provided substantial evidence that after annealing second phase particles become more organized and equiaxed. However, Fig. 4(a-b) clearly apparent the formation of PFZ along with unorganized patches of dispersed precipitates. On the contrary, in the annealed condition, the particles formed more orderly arranged 2D closed colonies of respective phases with the increase of annealing temperature. The inter-connected precipitated network consists of an alternative occurrence of Mg_2Si and $Al_6(Mn,Fe)$ layered structure. $Al_6(Mn,Fe)$ is a pre-existing phase for AA5XXX alloy series and considered as a good nucleation site for other hard β -phases like Mg_2Si (Engler and

Miller-Jupp, 2016; Engler *et al.*, 2017). In addition, it is also reported that $Al_6(Mn,Fe)$ stabilizes newly formed grain boundaries during annealing. For high Mg content alloys like AA5083, Al_6Mn is considered a most often getable phase where Fe content replaced some Mn atoms and formerly represented with $Al_6(Mn,Fe)$. It is depicted in Fig. 4(c-d) that samples annealed at 275 °C contained a high volume fraction of second phase particles with minimal inter precipitate distance. The alternate volume fractions of Mg_2Si and $Al_6(Mn,Fe)$ are clearly ascended up as annealing temperature upswings to 275 °C with a somewhat larger precipitate size in comparison to un-annealed state. Although, the globules of second phase particles are seeded in-between the grains as highlighted in Fig. 4(e) at 275 °C. Moreover, at 325 °C annealing temperature, the alternative occurrence density of

Mg₂Si has also increased along with Al₆(Mn,Fe) precipitates as shown in Fig. 4(e-f). It is also worthy to note that high-temperature annealing dissolved most of the globules of second phase particles that were present in the α -Al matrix in un-annealed state and 275 °C. Hence, annealing at high-temperature also provokes the dissolution of globular particles, thus forming an organized cluster of a ubiquitous array of Mg₂Si particles nucleated within pre-existed large constituents of Al₆(Mn,Fe) precipitates (Lin *et al.*, 2010; Engler *et al.*, 2013).

This resultant transformation has simultaneously declared improvement in tensile strength as previously reported in Fig. 2. The formed precipitates may strengthen up the alloy in two possible ways. First, by the formation of above reported hard β -phases and second by impeding the dislocation movement of primary phase atoms. The concluded trend in tensile properties in-between annealed and un-annealed samples is mainly due to the orderly arranged array of β -phase particles in the α -phase matrix. These orderly joined arrays would cause better dispersion strengthening within α -Al than scattered and separated β -phases in contrast with the un-annealed condition. The primary phase atoms would experience less retaliation during dislocation traveling in the un-annealed sample than in annealed samples, which causes gradual improvement in strength to 275 °C and 325 °C.

It is expected that different fracture zones exhibit different mechanical properties owing to the solidification morphology of weld beads. For understanding the fracture behavior of surface joints, pull-out tensile fracture specimens were detailed examined in Fig. 5(a-f). In fracture surface characterization three constituent zones are formed with similar patterns in all surface joints, which includes CFZ, BMFZ interface boundary and base material affected zones (BMAZ) as shown in Fig. 5a. Two fracture modes are categorically identified; define as Mode-I and Mode-II in CFZ and BMFZ respectively, which embraces the whole fracture mechanism. On the other hand, BMAZ is the transitional zone shown between BMFZ and BM region, which is an in-fact unfused zone that has no impact on joint strength. The CFZ which actually bears the tensile load consisted of 2-2.2 mm inside width on each welded side and comprises about approx. 40-45% of cross-section surface. Furthermore, the magnified interface boundary that separated the BMFZ and BMAZ is also highlighted in the same figure. In Fig. 5a, Section B represented the position of BMFZ interface boundary at the joint cross-section. Descriptively, the examination of the BMFZ interface boundary (Section C) is given in Fig. 5b. A band was created that consists of brittle intergranular fractured layers (Mode-II) propagated

towards downstream and terminated at the interface, which is considered as the extreme edge of the fused zone (BMFZ). In addition, multiple square-trapezoidal shaped micro serrated-facets fractured grains in-band region (blue color) were clearly visible at the intensified box. The details of Section A in Fig. 5a are thoroughly represented in Fig. 5(c-d) for the as surface-welded specimen. Upon solidification of the welding bead, the evidence of micro-voids cannot be neglected from the available fracture theories (Qiang and Wang, 2019), further evidence of presence is confirmed from the multiple highlighted patches of elongated micro-voids in Fig. 5c against the tensile load. The inside surfaces of micro-voids consists of serrated layers that tried to resist the detachment of solidified grain from the counter portion, however, ultimately failed due to 30-35 μ m in dimension. In Fig. 5(d) (CFZ), Mode-I is a predominant fracture mode, which includes dimples that were spread over the entire fractured surface leads to the confirmation of ductile fracture (Muzamil *et al.*, 2016). Moreover, at high magnification in Fig. 5d, small equi-sized fine fracture deep dimples existed, which shows the sign of shear-lips like necking to grains before fracture in the entire region (Huang *et al.*, 2018).

Furthermore, at multiple places, dimples were formed a collective fine flower type pattern considering of four-to-five elongated fracture grains across a center, which is a symbol of activated ductility. Due to low strength and resistivity at this stage, the grains were detached by forming a cluster where one grain trigger another. This type of observational fracture mode is clearly detectable in Fig. 5d for as surface-welded specimens. A similar shear-lips like the necking of each individual fractured grain is tangible in Fig. 5e for homogenize annealed case at 275 °C. The packets of equi-sized fractured dimples are separately marked in this figure. However, the endemic occurrence has shown more deep fractured dimples in contradict to the previous case in Fig. 5d that have been weighted as a radical contend for increment in joint strength. In addition, a significant transformation in the fracture morphology has been depicted in Fig. 5f for homogenize annealed specimen at 325 °C. The extra stretched dimples were shown the sign of shear fracture association within this treatment temperature (Tayebi *et al.*, 2019). The distributed packets of shear fracture as marked in Fig 5f are extremely helpful in providing the work-hardening effect and also improves the micro-plasticity (Muzamil *et al.*, 2019b) at localizing areas of surface welded joints. This combinative effect has depicted a typical reflection in terms of ultimate improvement in joint strength at 325 °C.

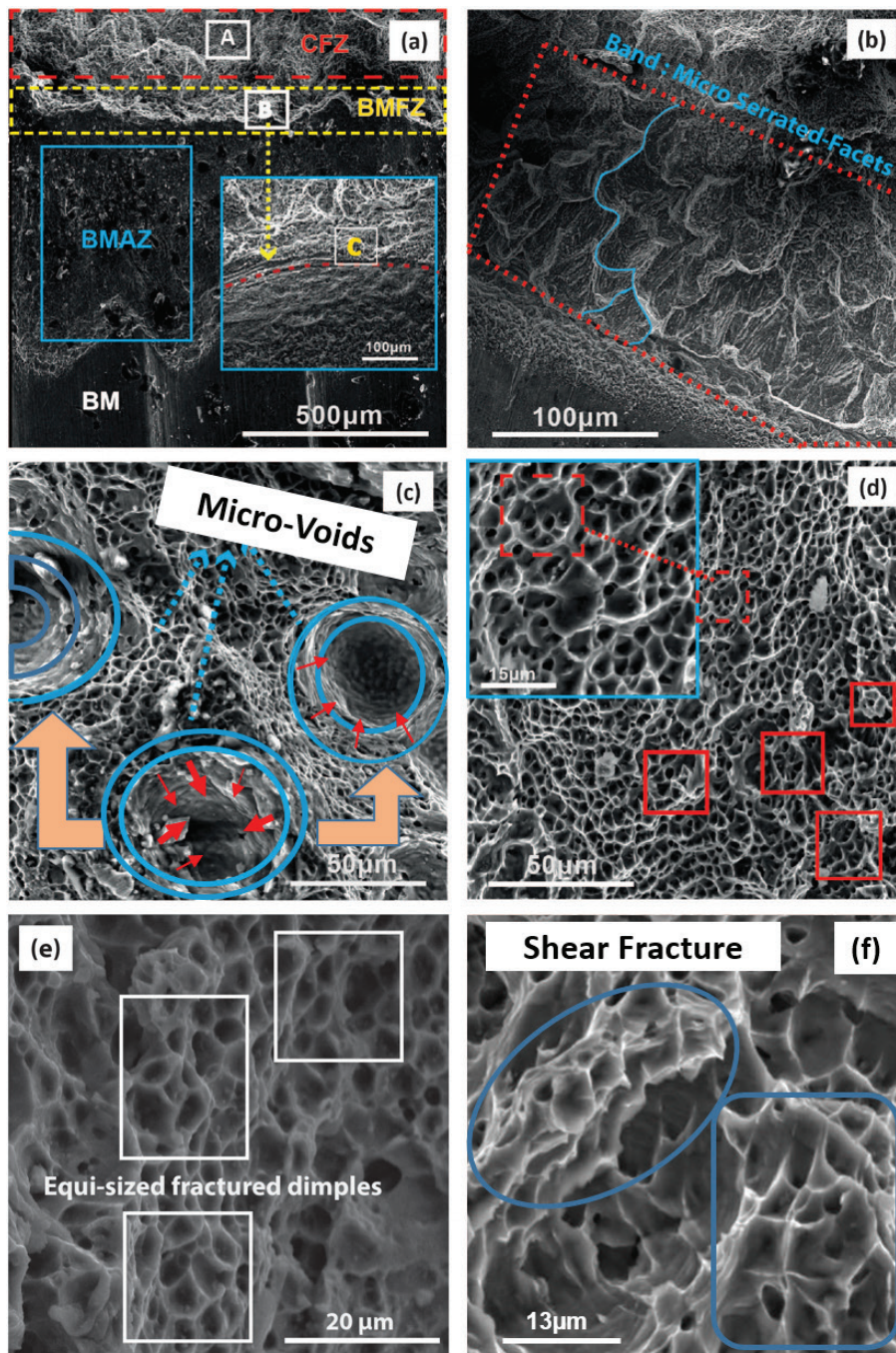


FIGURE 5. (a) Macro fracture surface of TIG welded surface joint, (b) details of Section C (BMFZ) interface boundary (Mode-II), (c) fracture surface details in Section A, (d) details at high magnification of Section A (CFZ) (Mode-I) of as-surface welded specimen, (e) details of (CFZ) Section A at 275 °C, and (f) details of (CFZ) Section A at 325 °C.

4. CONCLUSIONS

A new design and technique of surface welded joints were experimentally presented using tungsten inert gas welding process and the following conclusions have drawn:

- Homogenization annealing has been proven as a beneficial single-stage post-treatment operation for fusion-welded surface joints to gain up-trust in strength.
- Acceptable stress values, 162 and 197 MPa, were obtained for engineering applications by

- considering the cost of the welding process, efficiency and customer requirements for light-weight alloys.
- Microstructure analysis depicted the 2D closed colonies that were consisted of the alternative occurrence of Mg₂Si and Al₆(Mn,Fe). This layered structure density gradually upsurges along with precipitation size due to an increase in homogenization annealing temperature from 275 °C to 325 °C.
 - The fracture surfaces of joints have two distinct characteristics include; CFZ and BMFZ interface boundary. Against tensile load, CFZ bears the complete load and fractured in ductile deep dimples (Mode-I) which further transmits the load to BMFZ which formed a brittle transgranular band consisted of micro serrated-facets (Mode-II).

ACKNOWLEDGMENTS

The authors would like to provide special thanks to all the team members of the lab, School of Mechanical Engineering, Northwestern Polytechnical University, Xi'an, People's Republic of China for the on-time execution of work. Authors are also indebted of Shaanxi Materials Analysis and Research Center (SMARC), Northwestern Polytechnical University, for providing support in the post-experimental analysis.

REFERENCES

- Ahmadi, E., Ranjkesh, M., Mansoori, E., Fattahi, M., Mojalal, R.Y., Amirkhanlou, S. (2017). Microstructure and mechanical properties of Al/ZrC/TiC hybrid nanocomposite filler metals of tungsten inert gas welding fabricated by accumulative roll bonding. *J. Manuf. Process.* 26, 173–177. <https://doi.org/10.1016/j.jmapro.2017.02.012>.
- Baskutis, S., Baskutiene, J., Bendikiene, R., Ciuplys, A. (2019). Effect of weld parameters on mechanical properties and tensile behavior of tungsten inert gas welded AW6082-T6 aluminum alloy. *J. Mech. Sci. Technol.* 33, 765–772.
- Bozzi, S., Helbert-Etter, A.L., Baudin, T., Klosek, V., Kerbiguet, J.G., Criqui, B. (2010). Influence of FSSW parameters on fracture mechanisms of 5182 aluminium welds. *J. Mater. Process. Tech.* 210 (11), 1429–1435. <https://doi.org/10.1016/j.jmatprotec.2010.03.022>.
- Chen, R.-Y., Chu, H.-Y., Lai, C.-C., Wu, C.-T. (2015). Effects of annealing temperature on the mechanical properties and sensitization of 5083-H116 aluminum alloy. *Proc. Inst. Mech. Eng. Pt. L J. Mater.* 229 (4), 339–346. <https://doi.org/10.1177/1464420713512249>.
- D'Antuono, D.S., Gaies, J., Golumbfskie, W., Taheri, M.L. (2017). Direct measurement of the effect of cold rolling on β phase precipitation kinetics in 5xxx series aluminum alloys. *Acta Mater.* 123, 264–271. <https://doi.org/10.1016/j.actamat.2016.10.060>.
- Dolić, N., Brodarac, Z.Z. (2017). Evaluation of EN AW-5083 aluminum alloy homogeneity using statistical analysis of mechanical properties. *J. Min. Metall. Sect. B-Metall.* 53 (3), 429–439.
- Engler, O., Liu, Z., Kuhnke, K. (2013). Impact of homogenization on particles in the Al–Mg–Mn alloy AA 5454 – Experiment and simulation. *J. Alloys Compd.* 560, 111–122. <https://doi.org/10.1016/j.jallcom.2013.01.163>.
- Engler, O., Miller-Jupp, S. (2016). Control of second-phase particles in the Al–Mg–Mn alloy AA 5083. *J. Alloys Compd.* 689, 998–1010. <https://doi.org/10.1016/j.jallcom.2016.08.070>.
- Engler, O., Kuhnke, K., Hasenclever, J. (2017). Development of intermetallic particles during solidification and homogenization of two AA 5xxx series Al–Mg alloys with different Mg contents. *J. Alloys Compd.* 728, 669–681. <https://doi.org/10.1016/j.jallcom.2017.09.060>.
- Geng, S., Jiang, P., Shao, X., Mi, G., Wu, H., Ai, Y., Wang, Ch., Han, Ch., Chen, R., Liu, W. (2018). Comparison of solidification cracking susceptibility between Al–Mg and Al–Cu alloys during welding: A phase-field study. *Scripta Mater.* 150, 120–124. <https://doi.org/10.1016/j.scriptamat.2018.03.013>.
- Huang, Y., Li, Y., Xiao, Z., Liu, Y., Huang, Y., Ren, X. (2016). Effect of homogenization on the corrosion behavior of 5083-H321 aluminum alloy. *J. Alloys Compd.* 673, 73–79. <https://doi.org/10.1016/j.jallcom.2016.02.228>.
- Huang, Y., Lv, Z., Wan, L., Shen, J., dos Santos, J.F. (2017). A new method of hybrid friction stir welding assisted by friction surfacing for joining dissimilar Ti/Al alloy. *Mater. Lett.* 207, 172–175. <https://doi.org/10.1016/j.matlet.2017.07.081>.
- Huang, L., Wu, D., Hua, X., Liu, S., Jiang, Z., Li, F., Wang, H., Shi, S. (2018). Effect of the welding direction on the microstructural characterization in fiber laser-GMAW hybrid welding of 5083 aluminum alloy. *J. Manuf. Process.* 31, 514–522. <https://doi.org/10.1016/j.jmapro.2017.12.010>.
- Huh, M.Y., Cho, S.Y., Engler, O. (2001). Randomization of the annealing texture in aluminum 5182 sheet by cross-rolling. *Mat. Sci. Eng. A* 315 (1–2), 35–46. [https://doi.org/10.1016/S0921-5093\(01\)01207-2](https://doi.org/10.1016/S0921-5093(01)01207-2).
- Kumar, A., Sundarajan, S. (2009). Optimization of pulsed TIG welding process parameters on mechanical properties of AA 5456 Aluminum alloy weldments. *Mater. Design* 30 (4), 1288–1297. <https://doi.org/10.1016/j.matdes.2008.06.055>.
- Li, J., Carsley, J.E., Stoughton, T.B., Hector Jr, L.G., Hu, S.J. (2013). Forming limit analysis for two-stage forming of 5182-O aluminum sheet with intermediate annealing. *Int. J. Plasticity* 45, 21–43. <https://doi.org/10.1016/j.ijplas.2012.10.004>.
- Lin, S., Nie, Z., Huang, H., Li, B. (2010). Annealing behavior of a modified 5083 aluminum alloy. *Mater. Design* 31 (3), 1607–1612. <https://doi.org/10.1016/j.matdes.2009.09.004>.
- Muzamil, M., Akhtar, M., Samiuddin, M., Mehdi, M. (2016). Effect of heat treatment on impact resistance of AU₃GT and AS₃G06 aluminum alloys. *J. Mech. Sci. Technol.* 30 (10), 4543–4548. <https://doi.org/10.1007/s12206-016-0924-9>.
- Muzamil, M., Wu, J., Samiuddin, M., Majeed, A., Zhang, Z. (2019a). The response of heat-treatable filler on non-heat-treatable aluminum alloy substrate against age hardening cycle for intelligent development of surface welded joints using TIG welding process. *J. Braz. Soc. Mech. Sci. Eng.* 41 (5), 229. <https://doi.org/10.1007/s40430-019-1731-x>.
- Muzamil, M., Wu, J., Akhtar, M., Zhang, Z., Majeed, A., Yang, J. (2019b). Modified TIG welding joint process: An approach to improve microstructure and fracto-mechanical behavior by MWCNTs inducement in Al–Mg–Si alloy. *Materials* 12 (9), 1441. <https://doi.org/10.3390/ma12091441>.
- Palanivel, R., Mathews, P.K., Dinaharan, I., Murugan, N. (2014). Mechanical and metallurgical properties of dissimilar friction stir welded AA5083-H111 and AA6351-T6 aluminum alloys. *T. Nonferr. Metal. Soc. China* 24 (1), 58–65. [https://doi.org/10.1016/S1003-6326\(14\)63028-4](https://doi.org/10.1016/S1003-6326(14)63028-4).
- Qiang, W., Wang, K. (2019). Double-sided coaxial GTA flat-overhead welding of 5083 aluminum alloy. *J. Mater. Process. Tech.* 272, 9–16. <https://doi.org/10.1016/j.jmatprotec.2019.04.042>.
- Radetić, T., Popović, M., Romhanji, E. (2012). Microstructure evolution of a modified AA5083 aluminum alloy during a multistage homogenization treatment. *Mater. Charact.* 65, 16–27. <https://doi.org/10.1016/j.matchar.2011.12.006>.
- Ratchev, P., Verlinden, B., Van Houtte, P. (1995). Effect of pre-heat temperature on the orientation relationship of (Mn,Fe) Al₆ precipitates in an AA 5182 Aluminium–Magnesium

- alloy. *Acta Metall. Mater.* 43 (2), 621–629. [https://doi.org/10.1016/0956-7151\(94\)00261-F](https://doi.org/10.1016/0956-7151(94)00261-F).
- Samiuddin, M., Li, J.L., Taimoor, M., Siddiqui, M.N., Siddiqui, S.U., Xiong, J.T. (2020). Investigation on the process parameters of TIG-welded aluminum alloy through mechanical and microstructural characterization. *Def. Technol.* In Press. <https://doi.org/10.1016/j.dt.2020.06.012>.
- Soysal, T., Kou, S. (2019). Effect of filler metals on solidification cracking susceptibility of Al alloys 2024 and 6061. *J. Mater. Process. Tech.* 266, 421–428. <https://doi.org/10.1016/j.jmatprotec.2018.11.022>.
- Tayebi, P., Fazli, A., Asadi, P., Soltanpour, M. (2019). Formability analysis of dissimilar friction stir welded AA 6061 and AA 5083 blanks by SPIF process. *CIRP J. Manuf. Sci. Tech.* 25, 50–68. <https://doi.org/10.1016/j.cirpj.2019.02.002>.
- Vargas-Arista, B., Mendoza-Camargo, O., Zaragoza-Rivera, I.P., Medina-Flores, A., Cuevas-Salgado, E., Garfias-García, F., García-Vázquez, F. (2019). Influence of heat input on the Charpy ductile fracture behavior of reheated HAZ in GMAW multilayer welded joints on HSLA steel using digital fractographic analysis. *Rev. Metal.* 55 (2), e143. <https://doi.org/10.3989/revmetalm.143>.
- Xia, S.L., Ma, M., Zhang, J.X., Wang, W.X., Liu, W.C. (2014). Effect of heating rate on the microstructure, texture and tensile properties of continuous cast AA 5083 aluminum alloy. *Mat. Sci. Eng. A* 609, 168–176. <https://doi.org/10.1016/j.msea.2014.05.002>.
- Yi, G., Sun, B., Poplawsky, J. D., Zhu, Y., Free, M.L. (2018). Investigation of pre-existing particles in Al 5083 alloys. *J. Alloys Compd.* 740, 461–469. <https://doi.org/10.1016/j.jallcom.2017.12.329>.
- Zhang, J.X., Ma, M., Liu, W.C. (2017). Effect of initial grain size on the recrystallization and recrystallization texture of cold-rolled AA 5182 aluminum alloy. *Mat. Sci. Eng. A* 690, 233–243. <https://doi.org/10.1016/J.MSEA.2017.03.015>.